Supplementary Information for:

Active tuning of directional scattering by combining magneto-optical effects and multipolar interferences

M. Q. Liu, C. Y. Zhao* and B. X. Wang

Institute of Engineering Thermophysics, School of Mechanical Engineering, Shanghai Jiao Tong University, Shanghai 200240, China
*Corresponding author. E-mail: Changying.zhao@sjtu.edu.cn

Table of contents

1. Mie theory for a multilayer MO cylinder for section 3

As for magneto-optical materials considered in the work, the permittivity and permeability become anisotropic in the presence of an external magnetic field **B** and read[1]

$$\varepsilon_l \varepsilon_0 = \begin{pmatrix} \varepsilon_l & i\gamma_l & 0 \\ -i\gamma_l & \varepsilon_l & 0 \\ 0 & 0 & \varepsilon_{zl} \end{pmatrix} \varepsilon_0 \tag{s1}$$

$$\mu_l \mu_0 = \begin{pmatrix} \mu_l & i\eta_l & 0 \\ -i\eta_l & \mu_l & 0 \\ 0 & 0 & \mu_{zl} \end{pmatrix} \mu_0 \tag{s2}$$

where ε_0 and μ_0 are the permittivity and permeability in vacuum. The off-diagonal term γ_l and μ_l known as the Voigt parameters have dispersive characters and depend on an external DC magnetic field **B**. As shown in Fig. S1, without losing generality, here we consider a cylinder composed of multilayer magneto-optical materials. The incident plane wave is propagating along the x axis considering both *s* and *p* polarizations. Thus, the electromagnetic response can be analyzed based on generalized Mie theory[2].

For p-polarized waves in cylindrical coordinate system (r, ϕ, z), the incident field satisfy $E_i = E_0 \hat{y} e^{kr\cos\phi}$ and $H_i = H_0 \hat{z} e^{kr\cos\phi}$ with $E_0 = H_0 \sqrt{\varepsilon_0/\mu_0}$ where E_0 and H_0 are the electric and magnetic amplitudes. By expanding the electromagnetic fields into superposition of cylindrical harmonics, for $r > r_N$ where r_N is the radius of outer layer of cylinder, we can easily obtain $E_{sr} = -\sum\limits_{n=-\infty}^{\infty} E_n a_n n H_n(kr) e^{in\phi}/(kr)$,

$E_{s\phi} = -i \sum\limits_{n=-\infty}^{\infty} E_n a_n H_n'(kr) e^{in\phi}$ and $H_{sz} = \sum\limits_{n=-\infty}^{\infty} H_n a_n H_n(kr) e^{in\phi}$, where $E_n(H_n) = (-i)^n E_0(H_0)$, a_n is the Lorenz-Mie coefficients in scattering far-field and H_n is the first kind of Hankel functions. For multilayer cylinder with anisotropic materials, the field in the layer l should be modified and can be presented by[3-5]

$$\sum_{n=-\infty}^{\infty} \tag{s3}$$

$$\sum_{n=-\infty}^{\infty} \tag{s4}$$

$$\sum_{n=-\infty}^{\infty} \tag{s5}$$

where τ_n^l and ρ_n^l are the n-th mode coefficients in the l-th layer which could be found

by imposing the boundary conditions for the tangential components of the field H_{lz}^p and $E_{l\phi}^p$. Specially, for the sake of simplicity, we define

$$T_n\left(k_l^p r, \beta_l^p\right) = J_n'\left(k_l^p r\right) + \beta_l^p n J_n(k_l^p r)/(k_l^p r), \qquad \tilde{T}\left(k_l^p r, \beta_l^p\right) = \beta_l^p J_n' + n J_n(k_l r)/(k_l r),$$

$$Y\left(k_l^p r, \beta_l^p\right) = Y_n'\left(k_l^p r\right) + \beta_l^p n Y_n(k_l^p r)/(k_l^p r) \text{ and } \tilde{Y}\left(k_l^p r, \beta_l^p\right) = \beta_l^p Y_n'\left(k_l^p r\right) + n Y_n(k_l^p r)/(k_l^p r),$$

in which Y_n is the cylindrical Neumann function, and $k_l^p = \sqrt{\omega^2 \varepsilon_l^p \mu_l^p}$. In particular, for p-polarization, β_l^p equals to $\beta_l^p = \dfrac{\gamma_l}{\varepsilon_l}$ and $\mu_l^p = \mu_{lz}$, $\varepsilon_l^p = \varepsilon_l\left(1 - (\beta_l^p)^2\right)$. Additionally, we set $\rho_n^1 = 0$ to avoid the singularity of the Neumann functions at the cylinder axis. As such, the electromagnetic response of the multilayer MO cylinder can be obtained analytically.

As a result, in terms of the coated magneto-optical cylinder considered in our work, the corresponding Lorenz-Mie coefficients can be expressed as

$$a_n = \frac{\tilde{m}_s J_n'(x_s)\left[J_n(m_s x_s) - A_n Y_n(m_s x_s)\right] - J_n(x_s)\alpha_n}{\tilde{m}_s H_n'(x_s)\left[J_n(m_s x_s) - A_n Y_n(m_s x_s)\right] - H_n(x_s)\alpha_n} \tag{s6}$$

$$\tau_n^c = \frac{\tilde{m}_s c_n\left[J_n(m_s x_s) - A_n Y_n(m_s x_c)\right]}{\tilde{m}_c J_n(m_c x_c)} \tag{s7}$$

$$\tau_n^s = \frac{\dfrac{2i}{\pi x_s}}{\tilde{m}_s H_n'(x_s)\left[J_n(m_s x_s) - A_n Y_n(m_s x_s)\right] - H_n(x_s)\alpha_n} \tag{s8}$$

$$\rho_n^c = 0, \ \rho_n^s = -A_n \tau_n^s, \tag{s9}$$

in which the auxiliary functions are

$$\alpha_n = J_n(m_s x_s, \beta_s) - A_n Y_s(m_s x_s, \beta_s), \tag{s10}$$

$$A_n = \frac{\tilde{m}_c J_n(m_c x_c) J_n(m_s x_s, \beta_s) - \tilde{m}_s J_n(m_c x_c, \beta_c) J_n(m_s x_c)}{\tilde{m}_c J_n(m_c x_c) Y_n(m_s x_s, \beta_s) - \tilde{m}_s J_n(m_c x_c, \beta_c) Y_n(m_s x_c)}, \tag{s11}$$

with the size parameters $x_{c,s} = k_{c,s} r_{c,s}$. The superscripts c and s represent the core and shell. The relative refractive and impedance indices read $m_{c,s} = \sqrt{\varepsilon_{c,s}\mu_{c,s}/(\varepsilon_0\mu_0)}$ and $\tilde{m}_{c,s} = \sqrt{\varepsilon_{c,s}\mu_0/(\varepsilon_0\mu_{c,s})}$. Note that, if $\gamma_{c,s} = 0$ where the materials of core and shell are isotropic[6,7], the Eq. s11 will be equal to zero, and the results of Eq. s6-s9 are consistent

with those of an isotropic multilayer cylinder[1]. And the parity symmetry $a_{-n} = a_n$ and $\tau_n^l = \tau_{-n}^l$, $\rho_n^l = \rho_{-n}^l$ will hold at the same time.

For *s*-polarization, the incident fields satisfy $E_i = E_0 \hat{z} e^{krcos\phi}$ and $H_i = H_0 \hat{y} e^{krcos\phi}$. The scattering coefficients, including a_n, τ_n, ρ_n, can be easily obtained by replacing ($E_{lr}^p, E_{l\phi}^p, H_{lz}^p$) of *p*-polarization with $F(H_{lr}^s, H_{l\phi}^s, E_{lz}^s)$ where $F = \omega \mu_l^p / k_l^p$ for Eq. s3-s11. Besides, ($\varepsilon_l^p, \mu_l^p, \beta_l^p$) should be replaced by ($\varepsilon_l^s, \mu_l^s, \beta_l^s$) where $\varepsilon_l^s = \varepsilon_{lz}$, $\beta_l^s = \eta_l / \mu_l$ and $\mu_l^s = \mu_l (1 - (\beta_l^p)^2)$. The detailed derivation for a core-shell structure can be found in Ref. 4.

With the scattering coefficients in the hand, the scattering efficiency Q_{sca}, the scattering asymmetry parameter g and the field distributions can be easily obtained.

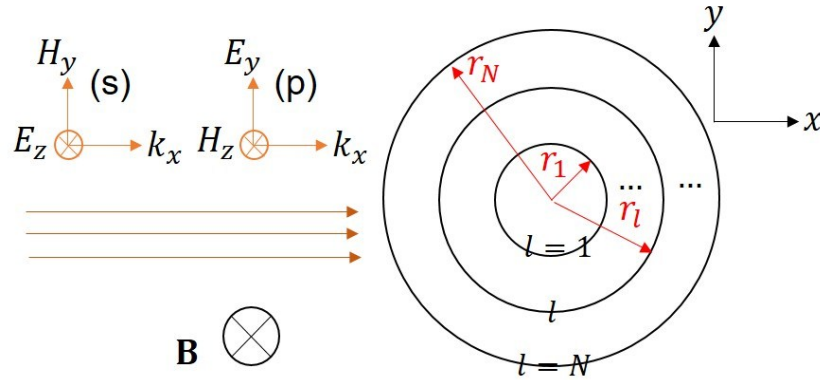Fig. S1 Schematic of the multilayer magneto-cylinder with p- and s-polarization. The direction of an external DC magnetic field **B** is along the axis of cylinder.

4

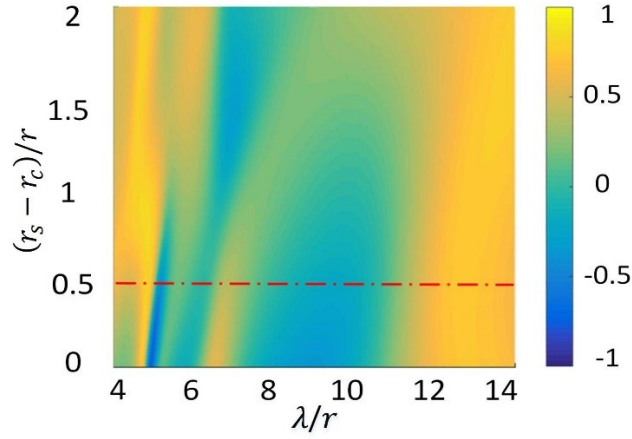## 2. Supplemental Fig. S2 and Fig. S3 for Section 3.1

Fig. S2 The result of scattering asymmetry parameter g as a function of normalized wavelengths λ/r and the thickness $(r_s - r_c)/r$ of the magneto-optical shell under p-polarization. The red line indicates that the scattering direction will be mainly forward when the thickness of the shell is large.
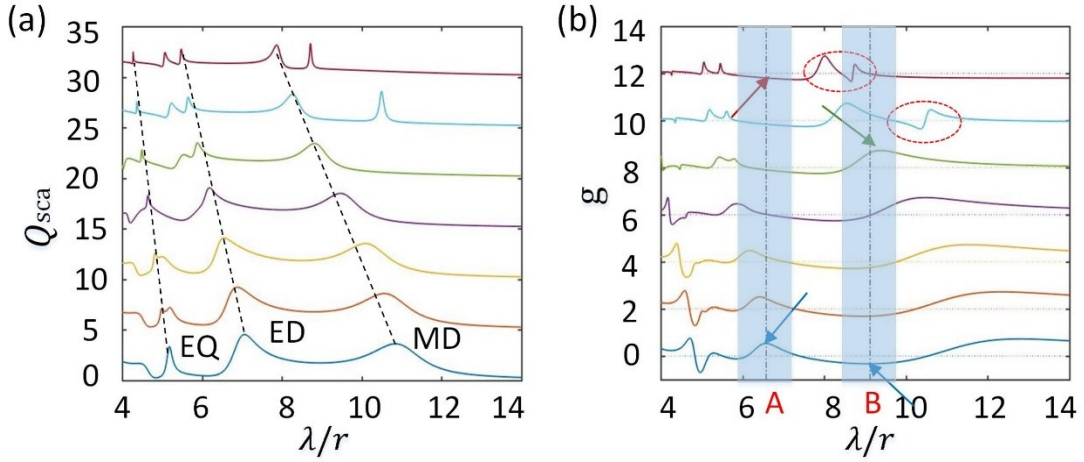

Fig. S3 **(a)** The scattering efficiency spectra Q_{sca} for representative values of γ_s under p-polarization. With each increase of γ_s, curves are shifted vertically by 5 for better separation. Three typical resonances are denoted and all the resonance positions are blue-shifted obviously. **(b)** The results of scattering asymmetry parameter g for typical γ_s, curves are shifted vertically by 2 for better separation. The arrows marked at λ_A and λ_B represent the inversion processes between forward and backward scattering. The two ovals circled with red dotted lines suggest the appearance of Fano-like resonances.

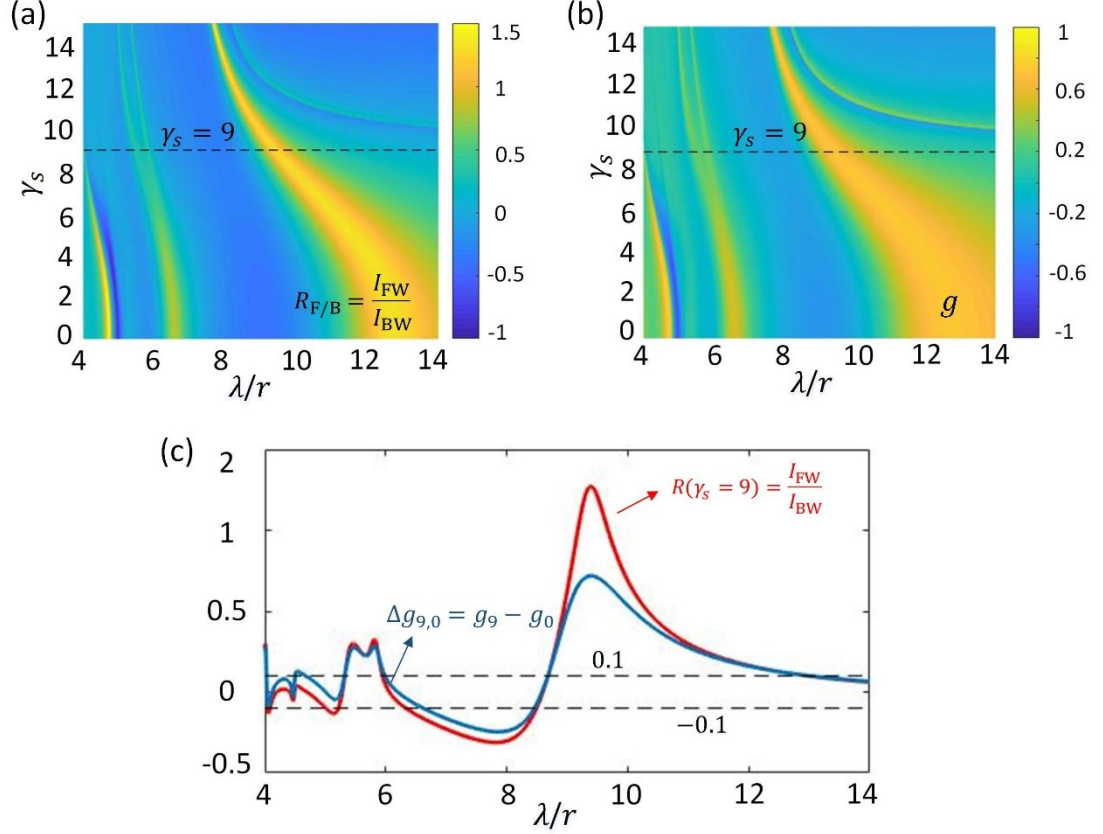## 3. Analysis of forward and backward scattering intensity for Section 3.3

Fig. S4 The results of **(a)** $\log_{10}(R_{F/B})$ and **(b)** scattering asymmetry parameter g as a function of γ_s and normalized wavelength λ/r. Two dotted lines in each subplot denoted with $\gamma_s = 9$ show the typical case. **(c)** The results of $R_{F/B}(\gamma_s = 9)$ and $\Delta g_{9,0}$. The dashed lines marked with ± 0.1 are denoted for better comparison.

Here, according to Mie theory, we define the scattering far-field intensity in forward ($\theta = -\dfrac{\pi}{2} \sim \dfrac{\pi}{2}$) and backward ($\theta = \dfrac{\pi}{2} \sim \dfrac{3\pi}{2}$) directions represented by

$$I_{FW} \sim \int_{-\pi/2}^{\pi/2} \left| \sum_{n=-\infty}^{\infty} a_n e^{in\theta} \right|^2 d\theta, \tag{s1}$$

$$I_{BW} \sim \int_{\pi/2}^{3\pi/2} \left| \sum_{n=-\infty}^{\infty} a_n e^{in\theta} \right|^2 d\theta \tag{s2}$$

in which a_n is the far-field scattering coefficients and θ is the scattering angle. Further, the ratio of scattering intensity in forward and backward half spaces is defined as

$$R_{F/B} = \frac{I_{FW}}{I_{BW}}. \qquad (s3)$$

As shown in Fig. S4(a) and S4(b), the spectra for $\log_{10} R_{F/B}$ and g are similar. It means that, on the one hand, the analysis of scattering asymmetry parameter in the main paper are reliable to measure the scattering distributions in forward and backward directions.

On the other hand, in Fig. S3(c), the results for typical case at $\gamma_s = 9$ show that the critical values $p = 0.1$ and $q = 2$ set in Section 3.3 for measuring the strength of optical switching are reasonable and acceptable, where the ratio between forward and backward scattering intensity is $R_{F/B} > 10^{0.1}$.
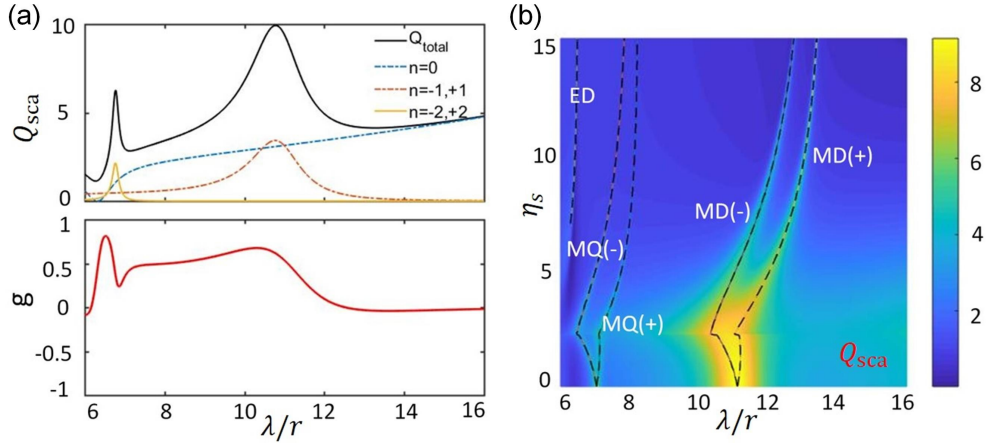
4. Supplemental Fig. S5 and Fig. S6 for Section 3.4

Fig. S5 **(a)** The scattering efficiency spectra Q_{sca} with multipolar contributions and the scattering asymmetric parameter g of the dielectric cylinder under $s-$ polarization. **(b)** The result of Q_{sca} as a function of normalized wavelength λ/r and Voigt parameter η_s for $s-$ polarization.
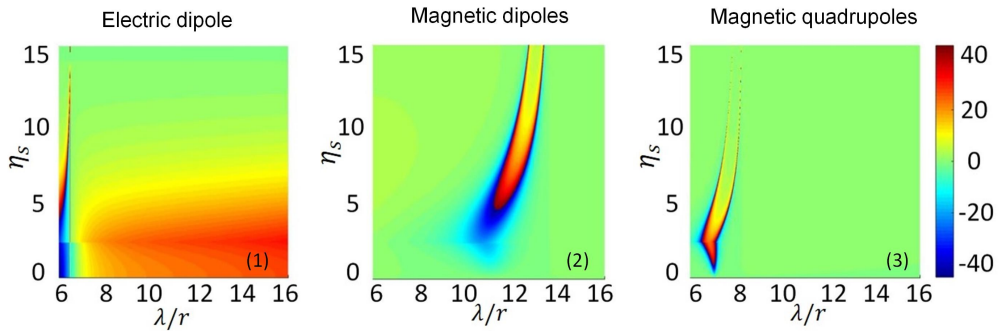
Fig. S6 The rotation angles for (1) ED, (2) MDs and (3) MQs with different operation wavelengths λ/r and Voigt parameter η_s for s − polarization.
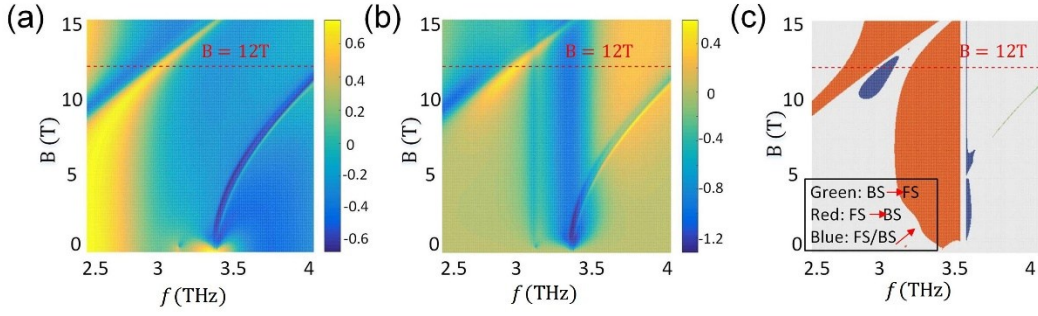
5. Supplemental Fig. S7 for Section 5

Fig. S7 The results of **(a)** the scattering asymmetry parameter g and **(b)** the strength of scattering inversion $\Delta g = g - g(B = 0)$ as a function of external magnetic intensity **B** and operation frequency f, along with the broadband areas satisfying the conditions with $p = 0.1$ and $q = 2$. The red regions indicate that the scattering direction can be altered from forward to backward, and the green region shows the opposite phenomena. The blue region represents that the directionality can be enhanced in the initial direction. The dotted lines marked in each figure show the typical case with $B = 12T$.

References

1. W. J. M. Kort-Kamp, F. S. S. Rosa, F. A. Pinheiro and C. Farina, *Phys. Rev. Lett.*, 2013, 111, 215504.
2. R. G. W. Brown, *Absorption and Scattering of Light by Small Particles*, Wiley, 1998, pp. 3–3(1).
3. W. J. M. Kort-Kamp, F. S. S. Rosa, F. A. Pinheiro and C. Farina, *J. Opt. Soc. Am. A*, 2014, 31, 1969–1976.
4. T. J. Arruda, A. S. Martinez and F. A. Pinheiro, Phys. Rev. A, 2016, 94, 033825.
5. A. Mirzaei, A. E. Miroshnichenko, I. V. Shadrivov and Y. S. Kivshar, *Scientific Reports*, 2015, 5, 9574.
6. T. J. Arruda and A. S. Martinez, *J. Opt. Soc. Am. A*, 2010, 27, 1679–1687.
7. T. J. Arruda, A. S. Martinez and F. A. Pinheiro, *J. Opt. Soc. Am. A*, 2014, 31, 1811–1819.